

Active Disturbance Rejection Control for Micro Air Vehicles Using Frequency Domain Analysis

Ulises Alvarez* Alicia Olascoaga* Diego Rivera*
A. Ramirez Mendoza* Octavio Garcia*
Luis Amezquita-Brooks*

* Universidad Autonoma de Nuevo Leon, Facultad de Ingenieria
Mecanica y Electrica

e-mail: ulises11590@gmail.com, altolascoaga@gmail.com, dndiego.23@gmail.com,
ameramirezme@conacyt.mx, octavio.garcias@uanl.mx,
luis.amezquitabr@uanl.edu.mx, abigail.ramirezmn@uanl.edu.mx,
ameramirezme@conacyt.mx

Abstract: Multi-rotor aerial vehicles, especially those of small size, are particularly susceptible to external perturbations, such as wind gusts. In this regard, Active Disturbance Rejection Control (ADRC) has been used successfully to reduce the effect of external perturbations for this kind of vehicle. Yet, in this paper, it is shown through frequency domain analysis that ADRC can be overly sensitive to sensor noise. Due to ADRC being based on state feedback control, determining performance and robustness specifications in the frequency domain is not straightforward. On the other hand, for output feedback control (OFC) there exists a comprehensive theoretical framework which allows to manage these parameters. Therefore, in this article a novel combination of classical OFC and ADRC is proposed. It is shown that using the proposed scheme, the nominal (i.e. without perturbation) characteristics of the control system can be defined exclusively by the OFC while the ADRC improves perturbation rejection. A drawback is that the resulting sensor noise sensitivity is degraded. In order to improve this parameter, the selection of proper observer gains for the ADRC observer and the use of a low-pass filtering element within the controller structure are studied. Finally, time domain simulations illustrate the effectivity of the proposed scheme.

Keywords: Disturbance Rejection, Sensitivity, Frequency Domain

1. INTRODUCTION

Micro air vehicles (MAV) such as quad-rotors, have become increasingly utilized in consumer and commercial applications. Today, many different control strategies have been successfully implemented, ranging from Proportional-Integral-Derivative (PID) controllers to non-linear methods such as sliding modes and backstepping (Zulu and John (2016)). Even though complex strategies have been successful, the prevalent control schemes are based on PIDs due to their relative simplicity and easy tuning. However, micro air vehicles are highly susceptible to disturbances due to wind gusts and/or plant uncertainties.

Active Disturbance Rejection Control (ADRC), introduced by Han in 1995 as an alternative to using conventional PID controllers, has been growing in popularity in several applications (Tian and Gao (2007)). The main advantage of ADRC is that it does not require an exact process model to estimate and compensate for disturbances. It is based on an extended state observer which models uncertainties and external perturbations as one large lumped disturbance. ADRC tuning has been refined and well documented, allowing a simpler implementation

(Chen et al. (2011)). Research has been conducted on different aspects of ADRC, such as frequency response analysis (Tian and Gao (2007)) of a linear representation of ADRC. In this context, the use of ADRC for improving the performance of MAV subject to perturbations is attractive, yet it has not been widely reported.

This aim of this study is to improve the disturbance rejection properties of a MAV subject to both input disturbances and sensor noise. In this sense, ADRC has been shown to be sensitive to sensor noise, a characteristic which is also confirmed here using frequency domain analysis. Therefore, a novel combination of a output feedback controller, designed using classical control theory, and ADRC is proposed. The main characteristics of this new scheme are presented. The resulting scheme provides a good combination of input perturbation and sensor noise rejection.

2. QUAD-ROTOR MODEL

The MAV can be modeled using Newton-Euler equations of motion and Fig. 1:

$$m\dot{V}_b + m\omega_b \times V_b = F_b \quad (1)$$

$$J\dot{\omega}_b + \omega_b \times (J\omega_b) = M_b \quad (2)$$

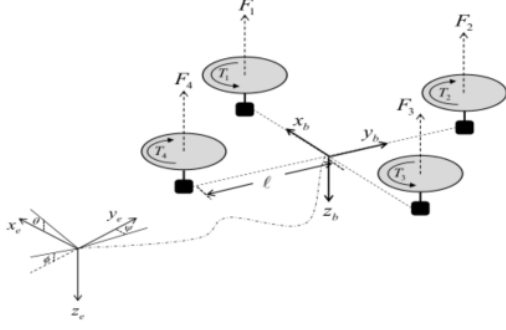


Fig. 1. Quadrotor frame and motor configuration (Gonzalez-Sanchez et al. (2013))

where $V_b = [u \ v \ w]^T$ and $\omega_b = [p_b \ q_b \ r_b]^T$ are the linear and angular velocity vectors, F_b is the external force vector, M is the mass, J is the inertial moment matrix, and M_b is the external moment vector. If the quad-rotor body is assumed to be symmetrical, then:

$$J = \text{diag}(I_\alpha, I_\alpha, I_z) \quad (3)$$

where I_α is the inertial mass along x and y axes, and I_z is the inertial mass along the z axis. Considering the Euler angles $\Omega = [\phi \ \theta \ \psi]^T$ with a rotation sequence $\psi - \theta - \phi$ (yaw-pitch-roll):

$$\omega_b = R_\alpha \dot{\Omega} \quad (4)$$

where:

$$R_\alpha^{-1} = \begin{bmatrix} 1 & s_\phi t_\theta & c_\phi t_\theta \\ 0 & c_\phi & -s_\phi \\ 0 & s_\phi/c_\theta & c_\phi/c_\theta \end{bmatrix}, \quad \Phi = [\phi \ 0 \ 0]^T \\ \Theta = [0 \ \theta \ 0]^T \\ \Psi = [0 \ 0 \ \psi]^T \quad (5)$$

$$s_x = \sin(x), \quad c_x = \cos(x), \quad t_x = \tan(x)$$

The thrust of the propeller can be approximated by:

$$F_i = k_p V_i^2 \quad (6)$$

where V is the voltage applied to the motor and k_p is a constant that can be experimentally characterized for each motor-propeller combination. Similarly, the reactive moment can be expressed as:

$$T_i = k_m V_i^2 \quad (7)$$

where k_m is a constant that can be that can be experimentally characterized as well.

The induced forces and moments due to thrust (6) and reactive moments (7) for an X type quadrotor are:

$$F_\alpha^b = [0 \ 0 \ F_z]^T \\ M_\alpha^b = [T_p \ T_q \ T_r]^T \quad (8)$$

where

$$\begin{bmatrix} F_z \\ T_p \\ T_q \\ T_r \end{bmatrix} = \begin{bmatrix} -k_p & -k_p & -k_p & -k_p \\ 0 & -\ell k_p & 0 & \ell k_p \\ \ell k_p & 0 & -\ell k_p & 0 \\ -k_m & k_m & -k_m & k_m \end{bmatrix} \begin{bmatrix} V_1^2 \\ V_2^2 \\ V_3^2 \\ V_4^2 \end{bmatrix} = P \begin{bmatrix} V_1^2 \\ V_2^2 \\ V_3^2 \\ V_4^2 \end{bmatrix} \quad (9)$$

Combining (8) and (4), we obtain the following simplified model (Bai et al. (2012)):

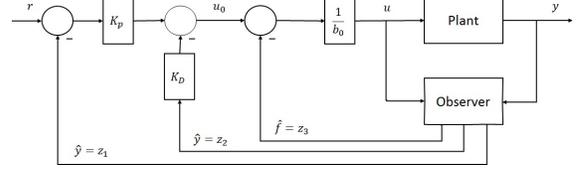


Fig. 2. Linear ADRC with complete state feedback

$$\ddot{\phi} = \dot{\theta} \dot{\psi} \left(\frac{I_\alpha - I_z}{I_\alpha} \right) + \frac{1}{I_\alpha} T_p \\ \ddot{\theta} = \dot{\phi} \dot{\psi} \left(\frac{I_z - I_\alpha}{I_\alpha} \right) + \frac{1}{I_\alpha} T_q \\ \ddot{\psi} = \dot{\phi} \dot{\theta} \left(\frac{I_\alpha - I_\alpha}{I_z} \right) + \frac{1}{I_z} T_r \quad (10)$$

In (Gonzalez-Sanchez et al. (2013), Bai et al. (2012)), the process for further simplification of the orientation model is shown. This results in the following transfer matrix:

$$G(s) = \text{diag} \left[\frac{1}{I_\alpha s^2} \quad \frac{1}{I_\alpha s^2} \quad \frac{1}{I_z s^2} \right] \quad (11)$$

In the following sections, this simplified model will be used for the design of several control schemes.

3. ACTIVE DISTURBANCE REJECTION CONTROL

Implementation of a second order ADRC has already been well studied (Herbst (2013), Chen et al. (2011), Tian and Gao (2007)). The central idea is to use an extended state observer (ESO) to estimate the internal and external disturbances in real time. Original ADRC has complex tuning parameters as well as nonlinear gains. However, (Gao (2006)) implemented ADRC using a linear observer, which simplified the implementation without compromising its performance and robustness.

A basic presentation of linear ADRC, as proposed by (Gao (2006)) is presented for a second-order system. A general second-order plant is considered as:

$$\ddot{y} = g(y, \dot{y}, w, t) + bu \quad (12)$$

where y is the system output, u is the control signal, b is a constant, and w represents external disturbances. ADRC treats $g(y, \dot{y}, w, t)$ as the generalized disturbance, which is denoted as $f(t)$. This generalized disturbance is estimated using an ESO. If $x_1 = y, x_2 = \dot{y}, x_3 = f$, the second-order plant can be represented with a state space model as shown below:

$$\dot{x} = Ax + Bu + Ef \\ y = Cx \quad (13)$$

where:

$$A = \begin{bmatrix} 0 & 1 & 0 \\ 0 & 0 & 1 \\ 0 & 0 & 0 \end{bmatrix}, \quad B = \begin{bmatrix} 0 \\ b \\ 0 \end{bmatrix} \quad E = \begin{bmatrix} 0 \\ 0 \\ 1 \end{bmatrix} \quad (14)$$

and $C = [1 \ 0 \ 0]$. Using the classical Luenberger equations for system (12), the ESO results in:

$$\dot{z} = Az + Bu + L(x_1 - z_1) \\ \hat{y} = Cz \quad (15)$$

where the observer gain vector L is chosen so that all the observer eigenvalues are located at $-\omega_0$ (Tian and Gao (2007)).

$$L = [3\omega_0 \ 3\omega_0^2 \ \omega_0^3]^T \quad (16)$$

If the observer is well tuned, it can be assumed that $z_1, z_2,$ and z_3 closely track $y, \dot{y},$ and f respectively. The control law

$$u = \frac{(u_0 - z_3)}{b} \quad (17)$$

reduces (12) to an approximated double integrator plant.

$$\ddot{y} = f + u_0 - z_3 \approx u_0 \quad (18)$$

The closed loop dynamics of (18) are then adjusted by using the complete state feedback:

$$u_0 = k_p(r - z_1) - k_d z_2 \quad (19)$$

where k_p and k_d are controller gains.

The use of ADRC imparts good input perturbation rejection characteristics and when no perturbation is present, the performance and robustness properties are the same as a typical state-feedback control.

Notwithstanding the attractive input perturbation rejection properties of ADRC, in the following sections it will be shown that the noise sensitivity of this scheme is high, limiting the usefulness of this scheme.

3.1 Classical Linear Control

It is well known that classical linear control, in particular if designed using frequency analysis tools, allows proper assessment of the robustness and performance. For instance, using the nominal system model (11), a set of linear controllers was designed using Bode shaping techniques for the pitch, roll, and yaw angles. The detailed design procedure for pitch and roll angles are presented as an example. The same procedure was utilized for the design of the yaw angle controller.

Due to the symmetry of the vehicle, the pitch and roll dynamics are similar, thus the same controller can be used for both. Controller (20) was designed for pitch and roll of the simplified model(11) considering the specifications in Table.1 and Table.2.

Table 1. Control Design Specifications

| | Specification | Proposed Control |
|-----------------------|---------------|------------------|
| Bandwidth | 2-10 rad/s | 5 rad/s |
| Phase Margin(M_p) | >60 deg | 78.6 deg |
| Gain Margin(M_g) | >12dB | -inf dB |

Table 2. Air Vehicle Parameters

| | |
|--------------------|---------------|
| Inertia I_α | .0049 kgm^2 |
| Inertia I_z | .0088 kgm^2 |
| b_α | 204.0816 |
| l | .225 m |

$$OFC(s) = \frac{1.225(s + 0.5)}{(s + 50)} \quad (20)$$

The nominal robustness and performance properties can be derived from the Bode plot shown in Fig. 3.

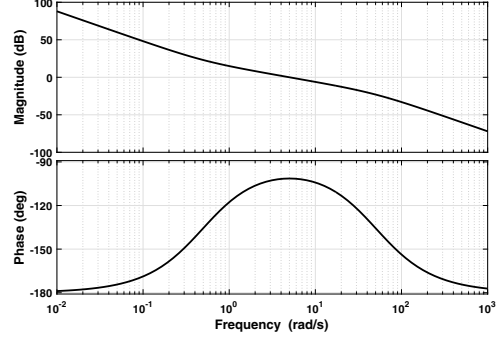


Fig. 3. Open loop Bode Plot pitch and roll dynamics using controller (20)

Designing a classical controller guarantees proper performance and robustness. However, it will be shown that this controller is highly sensitive to input disturbances. One method to improve this problem is to increase the controller gain at lower frequencies. Nonetheless, this would also introduce phase lag, which can compromise the robustness and transient responses (Lurie and Enright (2000)).

In the following sections a novel control scheme that combines the input disturbance properties of linear ADRC and the performance and robustness of classical control is presented.

3.2 A modified ADRC with classical control example

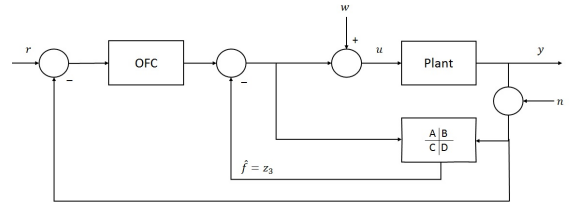


Fig. 4. Scheme combining OFC and ADRC

In contrast to the implementation of ADRC, only the estimation of the disturbance will be used in conjunction with a nominal control ($OFC(s)$) designed using frequency domain specifications. That is, the estimated lumped disturbance, z_3 , will be used in conjunction with the linear controller described in (20). The resulting scheme is shown in Fig. 4 and will be denoted as OFC+ADRC. The quadrotor model (11) is first expressed as a state space model. In this configuration, it is typical that two output variables are measured using an inertial measurement unit (IMU) to estimate angular positions. In particular, the accelerometer of an IMU are used to reconstruct angular position, while the gyroscopes measure angular velocities. Therefore, for the ADRC observer both outputs are used, while the linear controller OFC only utilizes angular position feedback.

$$\begin{pmatrix} \dot{x}_1(t) \\ \dot{x}_2(t) \\ \dot{x}_3(t) \end{pmatrix} = A \cdot \begin{pmatrix} x_1(t) \\ x_2(t) \\ x_3(t) \end{pmatrix} + B \cdot u(t) + E \cdot \dot{f}(t) \quad (21)$$

$$y(t) = C \cdot \begin{pmatrix} x_1(t) \\ x_2(t) \\ x_3(t) \end{pmatrix}$$

where

$$A = \begin{pmatrix} 0 & 1 & 0 \\ 0 & 0 & 1 \\ 0 & 0 & 0 \end{pmatrix}, B = \begin{pmatrix} 0 \\ b \\ 0 \end{pmatrix}, E = \begin{pmatrix} 0 \\ 0 \\ 1 \end{pmatrix} \quad (22)$$

$$C = \begin{pmatrix} 1 & 0 & 0 \\ 0 & 1 & 0 \end{pmatrix}$$

The resulting ESO is:

$$\dot{\hat{X}} = (A - LC)\hat{X} + [B \ L] \begin{bmatrix} u(t) \\ y(t) \\ \dot{y}(t) \end{bmatrix} \quad (23)$$

where $L = \begin{bmatrix} l_{11} & l_{12} \\ l_{21} & l_{22} \\ l_{31} & l_{32} \end{bmatrix}$

Summarily, the state space matrices of the ADRC observer yield:

$$A_{Obs} = \begin{bmatrix} -l_{11} & 1 - l_{12} & 0 \\ -l_{21} & -l_{22} & 1 \\ -l_{31} & -l_{32} & 0 \end{bmatrix}, B_{Obs} = \begin{bmatrix} 0 & l_{11} & l_{12} \\ b & l_{21} & l_{22} \\ 0 & l_{31} & l_{32} \end{bmatrix} \quad (24)$$

$$C_{Obs} = [0 \ 0 \ 1]$$

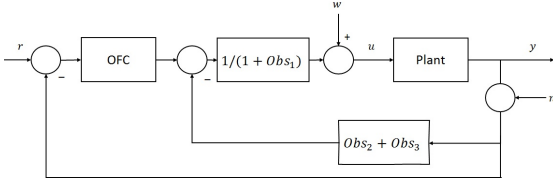


Fig. 5. Linear Control and ADRC

To analyze the effects of the coupling of ADRC with the linear controller, the Laplace transform of the state observer was taken. That is:

$$z_3(s) = C_{Obs}(sI - A_{Obs})B_{Obs} [u(s) \ y(s) \ \dot{y}(s)]^T \quad (25)$$

$$= [Obs_1 \ Obs_2 \ Obs_3] [u(s) \ y(s) \ \dot{y}(s)]^T$$

Making the proper block algebra simplifications, the final proposed control scheme is shown in Fig. 5, where:

$$Obs_1 = -\frac{b}{l_{32}} \frac{(s + (l_{31} + l_{11}l_{32} - l_{21}l_{31})l_{22})}{A_1} \quad (26)$$

$$Obs_2 = \frac{s \left(s + \frac{l_{22}l_{31} - l_{21}l_{32}}{l_{31}} \right)}{A_1}$$

$$Obs_3 = \frac{l_{32}s^2 + (l_{11}l_{32} - l_{12}l_{31})s + (l_{21}l_{32} - l_{22}l_{31})}{A_1}$$

and $A_1 = s^3 + (l_{11} + l_{22})s^2 + (l_{21} + l_{32} + l_{11}l_{22} + -l_{12}l_{21})s + (l_{31} + l_{11}l_{32} - l_{12}l_{31})$.

As follows it will be shown that in nominal conditions; without perturbation, the resulting closed loop response depends only on the linear controller (OFC(s)). This implies that the ADRC component does not affect the performance and robustness provided by the linear controller. According to Fig. 4, in nominal conditions, the resulting transfer function which models the closed loop response is given by:

$$\frac{y(s)}{r(s)} = \frac{OFC(s)Obs_{loop}(s)}{1 + OFC(s)Obs_{loop}(s)} \quad (27)$$

where

$$Obs_{loop}(s) = \frac{\frac{G(s)}{1+Obs_1}}{1 + \left(\frac{G(s)(Obs_2+Obs_3)}{1+Obs_1} \right)}$$

Substituting eq. (26) into (27) it turns out that:

$$\frac{y(s)}{r(s)} = \frac{OFC(s)G(s)}{1 + (OFC(s)G(s))} \quad (28)$$

which is equal to the closed loop transfer function if only the OFC controller is considered.

This is a key result as it shows that the effect of the ADRC observer is separable from any linear feedback controller in closed loop if only the perturbation rejection component of ADRC is used.

4. DISTURBANCE AND NOISE ANALYSIS

In this section, the main noise and disturbance rejection features of the OFC scheme, described in section 3.1, and the OFC+ADRC scheme, derived in section 3.2, will be compared in the frequency domain.

4.1 Pole Placement Analysis

In (Tian and Gao (2007)), a simple method for selecting the ADRC observer gains is presented. This method can be used when the measured variable is a scalar signal. However, due to the air vehicle system having a two dimensional measurement vector, the method proposed in (Tian and Gao (2007)) cannot be applied directly. Therefore, a pole placement algorithm was used to set the poles at different frequencies, as shown in Fig.6 and Fig.7.

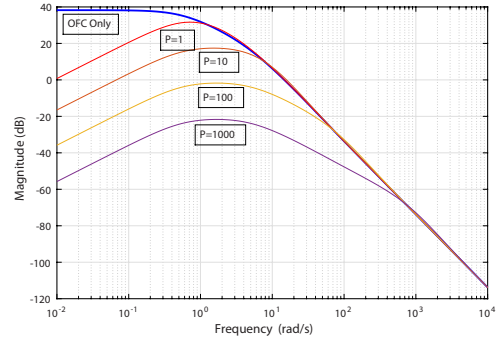


Fig. 6. Input Disturbance Sensitivity of $OFC(s)G(s)$ and $(OFC + ADRC)G(s)$

Fig. 6 shows the sensitivity to input disturbances of the OFC and OFC + ADRC control schemes. It is clear that the OFC + ADRC combination greatly improves the sensitivity to low frequency input disturbances compared to the standalone OFC scheme. In addition, it can be seen that as the observer poles increase the input disturbance sensitivity decreases. This result is in line with the expected behavior of the disturbance observer: increasing the observer performance improves the input disturbance rejection.

Fig. 7 shows the sensitivity to sensor noise of the OFC and OFC + ADRC control schemes. In contrast to the input

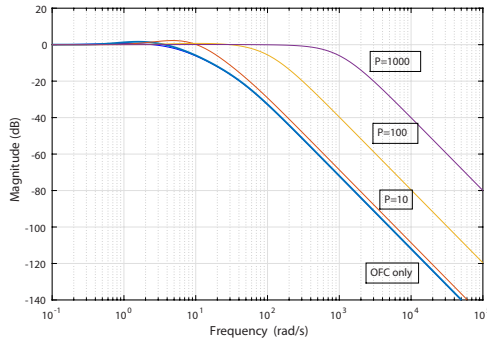


Fig. 7. Noise Sensitivity of $OFC(s)G(s)$ and $(OFC + ADRC)G(s)$

perturbation rejection, the system is more susceptible to high frequency sensor noise as the observer poles frequency increases. This higher sensitivity is especially detrimental as IMU measurements contain a significant amount of high frequency noise. Lowering ADRC observer pole values reduces noise sensitivity; however, the attractive input disturbance properties are negatively impacted.

4.2 Low Pass Filter-ADRC Combination

The previous results suggest that the selection of the ADRC observer gains should be made considering a compromise between sensor noise and input perturbation rejection. In current literature, there are several methods which could be potentially used for this purpose, such as optimal control theory. In the following section, a simple approach for adjusting the resulting sensor noise sensitivity is presented. This method is based on introducing a low pass filter within the ADRC transfer functions in order to cutoff the bandwidth of the observer. The resulting scheme is shown in Fig. 8.

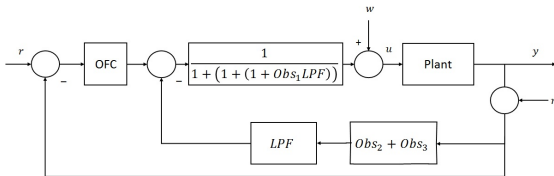


Fig. 8. OFC + ADRC with Low Pass Filter

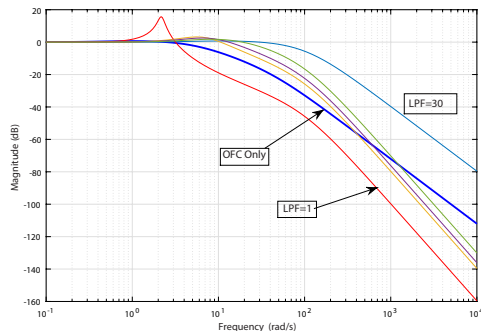


Fig. 9. Sensor Noise Sensitivity of $OFC(s)G(s)$ and $(OFC + ADRC + LPF)G(s)$

Fig. 9 shows the sensitivity to sensor noise of the OFC scheme compared to that of the OFC+ADRC using the proposed LPF. The filter cutoff frequencies considered are: $\omega_c = [1, 10, 15, 30]rad/s$. From this figure, it is clear that as the LPF cutoff frequency decreases, the sensor noise sensitivity improves.

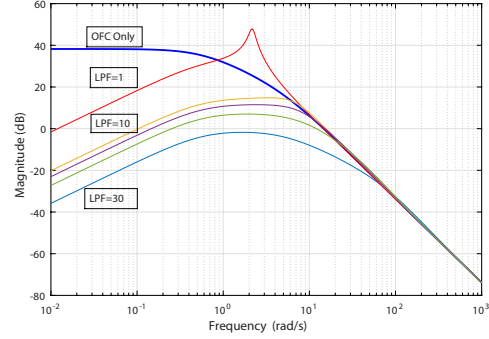


Fig. 10. Input Disturbance Sensitivity of OFC and OFC+ADRC using the LPF at several cut frequencies

On the other hand, the frequency of the LPF also affects the input disturbance rejection, as shown in Fig. 9. As the LPF cutoff frequency decreases, the input disturbance rejection deteriorates. Nonetheless, in all cases the input disturbance rejection at lower frequencies is significantly better than that of the OFC scheme.

An important observation from Figs. 9 and 10 is that for low ω_c values, the filter begins to interfere with the dynamics of $OFC(s)G(s)$, introducing a phase lag in the open loop transfer function, causing a large unwanted peak. This is also indicative of a reduced level of robustness. Therefore, a LPF cutoff frequency higher than the nominal open loop bandwidth is indicated in order to avoid this problem.

From Figs. 10 and 9, it can be concluded that adding a low pass filter adds a new parameter for tuning the level of ADRC disturbance rejection and sensor noise sensitivity, simplifying the task of achieving the required specifications. Although a similar result can be reached by proper tuning of the ADRC observer gains, the introduction of the LPF has a clear and unique effect, making it simpler to adjust. Finally, it should be noted that the proposed scheme allows achieving good levels of sensor noise and input perturbation rejection for high and low frequency bands respectively. However, the cross-over frequency band is still vulnerable to these perturbations. This is a well known limitation which applies to all control schemes (Lurie and Enright (2000)).

5. TIME DOMAIN SIMULATION EXAMPLES

A quadrotor simulation restricted to the the pitching moment was implemented to compare the different control schemes described in the previous section. The ADRC parameters used in the simulation are shown in Table. 3.

Table 3. Simulation Parameters

| ADRC Observer Poles | [100, 101, 102] |
|---------------------|-----------------|
| LPF ω_c | 15 rad/s |

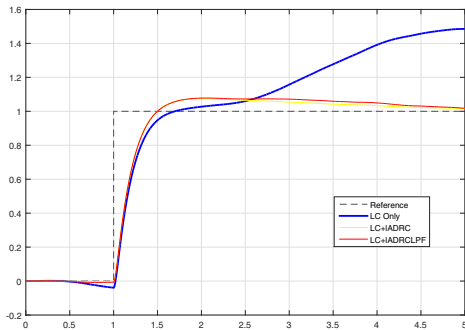


Fig. 11. Comparison of step response of the closed loop system with OFC, OFC+ADRC, and OFC + ADRC + LPF with low frequency input disturbances

Fig. 11 shows the step response of the three control schemes subjected to a pseudo-random low frequency input noise ($< 0.1 \text{ rad/s}$). It is clear that both OFC + ADRC and OFC + ADRC + LPF are effective in rejecting the low frequency input disturbances. In contrast, the OFC fails in this regard.

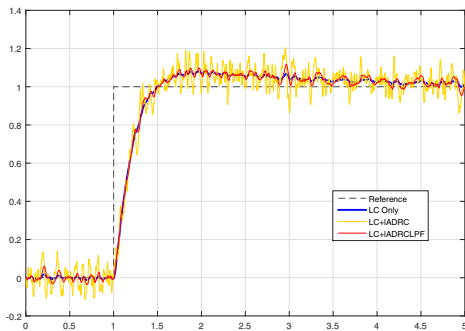


Fig. 12. Comparison of step response of the closed loop system with OFC, OFC+ADRC, and OFC + ADRC + LPF with high frequency sensor noise.

Fig. 12 shows the step response of the three control schemes subjected to high frequency pseudo-random sensor noise ($> 100 \text{ rad/s}$). As previously discussed, ADRC induces an increase in sensor noise sensitivity, which can be clearly seen. However, the addition of the LPF in the OFC + ADRC + LPF scheme greatly reduces this problem.

The simulations confirm that combining ADRC with OFC greatly improves the disturbance rejection properties of the resulting scheme, but this also exacerbates sensor noise. This problem can be ameliorated by adding a LPF within the ADRC structure, reducing sensor noise at a minimal cost of disturbance rejection performance.

6. CONCLUSION

In this article, the perturbation rejection and sensor noise characteristics of ADRC are analyzed in the frequency domain. It can be concluded that ADRC schemes can be overly sensitive to sensor noise, but in turn provide good perturbation rejection properties. On the other hand, it

is well known that classical control design allows a clear measurement of performance and robustness properties. This motivates the combination of an output feedback controller, designed using classical control elements, with an ADRC observer, intended to improve the input perturbation rejection. The proposed ADRC+OFC combination is shown to be separable if no input perturbation is present. Therefore, the nominal performance and robustness characteristics are completely defined by the OFC. However, if input perturbations are present, the ADRC observer is effective in rejecting said perturbations. A further analysis of the effects of sensor noise shows that, due to the ADRC observer, the sensor noise sensitivity is deteriorated. The study shows that this issue can be partially rectified by the proper selection of the ADRC observer gains. However, this problem has not been properly reported in the current literature. A simple proposal to address this problem is presented by introducing a low pass filter in key elements of the ADRC observer. The results show that this yields a control scheme easy to adjust using frequency domain elements. Finally, the results are validated in the time domain through digital simulations. The results encourage further study regarding the optimization of the ADRC observer gain and LPF tuning as well as experimental validation.

REFERENCES

- Bai, Y., Liu, H., Shi, Z., and Zhong, Y. (2012). Robust control of quadrotor unmanned air vehicles. In *Chinese Control Conference*, 4462–4467. IEEE.
- Chen, X., Li, D., Gao, Z., and , C.W. (2011). Tuning method for second-order active disturbance rejection control. In *Chinese Control Conference*, 6322–6327. IEEE.
- Gao, Z. (2006). Scaling and bandwidth-parameterization based controller tuning. In *Proceedings of the American control conference*, volume 6, 4989–4996.
- Gonzalez-Sanchez, M., Amezquita-Brooks, L., Liceaga-Castro, E., and Zambrano-Robledo, P. (2013). Simplifying quadrotor controllers by using simplified design models. In *Conference on Decision and Control*, 4236–4241. IEEE.
- Herbst, G. (2013). A simulative study on active disturbance rejection control (adrc) as a control tool for practitioners. *Electronics*, 2(3), 246–279.
- Lurie, B. and Enright, P. (2000). *Classical feedback control: with MATLAB*. CRC Press.
- Tian, G. and Gao, Z. (2007). Frequency response analysis of active disturbance rejection based control system. In *International Conference on Control Applications*, 1595–1599. IEEE.
- Zulu, A. and John, S. (2016). A review of control algorithms for autonomous quadrotors. *arXiv preprint arXiv:1602.02622*.